An Optical-Trap Force Transducer that Operates by Direct Measurement of Light Momentum

Steven B. Smith[4], Yujia Cui [5] and Carlos Bustamante[1-4]

[1]Department of Chemistry, [2]Department of Physics,

[3]Department of Molecular and Cell Biology,

[4]Howard Hughes Medical Institute,

University of California, Berkeley, CA: 94720-7300

[5] Department of Cellular and Molecular Pharmacology,
University of California, San Francisco, CA 94143-0450

submitted to ***Methods in Enzymology,*** **October 29, 2001**

Introduction

"Optical tweezers" is a name given by Arthur Ashkin and colleagues to a device they invented, which uses light pressure to manipulate tiny objects. By focusing a laser beam through a microscope objective, they found that particles with high indexes of refraction, such as glass, plastic, or oil droplets, were attracted to intense regions in the beam and could be held permanently at a focal point [1, 2]. Optical tweezers are useful in molecular and cell biology because several important forces are in an accessible picoNewton (pN) range; e.g. ligand / receptor binding, DNA stretching, protein unfolding, and molecular motor stall forces.

Several good reviews cover the physics of optical traps [3, 4] but briefly their operation can be explained in either of two ways. In the first, light impinging on the particle is seen to be refracted or reflected by that particle. Since light photons carry a momentum $\vec{\mathbf{P}} = \hbar\vec{k}$ (where $\hbar$ is Plank's constant and $\vec{k}$ is the wave vector), the particle feels a reaction impulse which is equal but opposite to the change in the photon's momentum. If a particle acts as a positive lens and refracts light photons in a direction towards the object's center, then that object will become entrained or trapped in a light beam, especially if the beam has a narrow waist or focal point. The second explanation applies to particles that are much smaller than a wavelength of light, and can thus be treated as a Rayleigh scatterer possessing a polarizability, α. The electric field E from a light source induces a dipole moment αE in the particle which experiences a force $\vec{\mathbf{F}} = \alpha/2 \nabla\vec{\mathbf{E}} \cdot \vec{\mathbf{E}}^*$ attracting it to the focus of the light. Since α is proportional to the particle volume, the force holding the particle in the trap is proportional to the particle size, as well as the beam intensity gradient.

Methods to measure such forces in the optical trap have been under continuous development. Most force-measurement methods treat the optical trap as a harmonic potential well or "virtual spring" that pulls the bead toward the trap center. By measuring the displacement Δx of the particle within the trap and estimating a spring constant κ, the force is then given by $F = \kappa\Delta x$. A spherical bead's position inside a trap can be measured with sub-nanometer precision by one of several optical methods, and so this technique has proven very effective [5, 6, 7].

Unfortunately, calibration of the virtual spring suffers from technical issues that complicate practical measurements. The particle-displacement sensor is often calibrated by translating a particle, fixed to a coverslip, by some known distance while measuring the response of a photodetector. However such calibration applies only to other particles having the same size, shape and orientation. Changes in the axial position (focal depth) of the particle can also affect the position-detector's sensitivity. Calibration of trap stiffness κ is usually done with a test force, either an externally applied drag force or thermal Brownian force. However, both the Stokes'-law drag and thermal corner-frequency methods require knowledge of the object's size and shape as well as the local fluid viscosity in order to obtain the particle's drag coefficient [3]. If the trapped particle is near a stationary surface, like a coverslip or cell wall, the particle' drag coefficient

increases[8]. Alternately, to estimate κ without using a drag coefficient, the equipartition theorem can be used to equate the particle's potential and thermal energies.

$$\tfrac{1}{2}\,\kappa\langle\Delta x^2\rangle = \tfrac{1}{2}\,k_B T \qquad (1)$$

This method requires accurate distance measurement at high bandwidth along an axis corresponding to a single degree of freedom. If the particle's axial position or angular orientation couple to the transverse distance detector, then more than one degree of freedom will be sampled and κ will be underestimated. This method is also susceptible to instrumental noise and bandwidth limitations [9].

Calibration problems can also arise when different particles are introduced into the trap or when optical conditions change. Then the shape of the potential well changes and κ must be re-calibrated for the new conditions. The trap stiffness is sensitive to the focal spot size and this, in turn, is affected by the spherical aberration of the objective lens. This aberration depends on the depth of the sample below the coverslip, so a calibration for κ performed 5 μm below the coverglass is invalid for experiments done at 10μm depth (except for water-immersion lenses). Although early studies have shown that arbitrary biological objects could be manipulated inside cells [10, 11], it has been much more difficult to estimate the forces generated by those objects because the stiffness of the virtual spring depends on the particle/light field interaction. This interaction, in turn, depends on the size and shape of the organelle, its index of refraction, and the refractive index of the cell's cytoplasm. Calibration is straightforward for plastic beads of reproducible size in a simple environment, but there is no practical way to transfer those beads (or their calibration) into the complex environment of the cell's interior. Therefore most molecular motor experiments are currently being done *in vitro*.

Here we present a new [12] force-measurement method, based on an opposed-beam optical tweezers design, which overcomes some of these limitations. By measuring the angular intensity distribution of the laser light as it enters and leaves the trap, it is possible to determine the change in the momentum flux of the light beam, which in turn, is strictly equal to the externally applied force on the particle. The force calibration now becomes independent of the particle's size, shape or refractive index, its distance beyond the coverslip (spherical aberration), the viscosity or refractive index of the buffer, and variations in laser power.

A light-momentum force sensor calibrated from first principles (conservation of linear momentum) was thus constructed and has been used in the following structural and enzyme studies: Stretching single DNA molecules [13], condensation of single DNA molecules [14], unfolding and refolding single titin molecules [15], mechanics of single RecA/DNA fibers [16], pulling single chromatin fibers [17], DNA polymerase activity vs. template tension [18], unfolding and refolding RNA structures [19], and phage packaging motor activity vs. force [20].

Force Sensor Theory

A device to measure light-momentum force is outlined in Fig. 1. Here light is shown entering from the left and being focused by an objective lens into a spot where a particle is trapped. Light that exits the trap toward the right is collected by a similar objective lens. If an external force is applied to the particle, the light is refracted asymmetrically by the particle and exits the trap with a modified angular distribution. A position-sensitive photo detector (far right) measures the power and offset of this light to infer the external force.

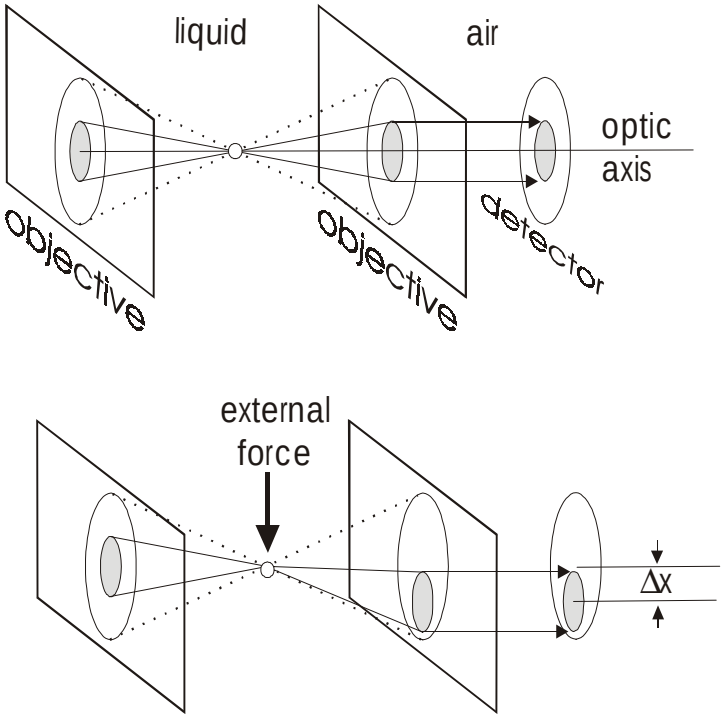

Figure 1. ***(Left)*** *Dashed lines indicate the outermost rays collected by an objective lens, defining the numerical aperture of the lens. The inner cone (solid lines) encloses the laser beam that enters from the left, passes through the bead, is imaged by the right objective and exits.* ***(Right)*** *Application of an external force to the bead will cause it to equilibrate slightly off center in the trap so that light pressure from the deflected beam exactly balances the external force. The angular deflection, θ, of a ray leaving the trap is transformed by the right objective into an offset distance, ΔX, such that* $\Delta X/R_L = n_l \sin(\theta)$ *where* n_l *is the refractive index of the liquid and* R_L *is the focal length of the lens. The transverse light force F felt by a bead as it deflects a light ray of intensity W through an angle θ is given by* $F = (n_l W/c) \sin(\theta)$ *where c is the speed of light.*

Therefore $F = (W/c)(\Delta X/R_L)$.

Consider light that is transmitted through a transparent liquid of refractive index n_l and which interacts with an object immersed in that liquid. A light wave carries with it a momentum flux given by [21]

$$d(d\vec{\mathbf{P}}/dt) = (n_l/c)\vec{\mathbf{S}}dA \qquad (2)$$

where $\vec{\mathbf{S}}$ is Poynting's vector, c is the speed of light, and dA is an element of area normal to $\vec{\mathbf{S}}$. The light force on the object is the difference in flux of the momentum entering ($\vec{\mathbf{P}}_{in}$) and leaving ($\vec{\mathbf{P}}_{out}$) the vicinity of the object. The force can be obtained by integrating the light intensity entering ($\vec{\mathbf{S}}_{in}$) and leaving ($\vec{\mathbf{S}}_{out}$) through a surface surrounding the object, provided elements of that surface (dA) are everywhere normal to $\vec{\mathrm{S}}$

$$\vec{\mathbf{F}} = d\vec{\mathbf{P}}_{in}/dt - d\vec{\mathbf{P}}_{out}/dt = (n_l/c)\iint(\vec{\mathbf{S}}_{in} - \vec{\mathbf{S}}_{out})dA \qquad (3)$$

For an optical trap, integration can be performed over a distant ($R>>\lambda$) spherical surface centered on the focal point. Here $\vec{\mathbf{S}}_{in}$ is normal to the surface because the incoming wave is spherical, and $\vec{\mathbf{S}}_{out}$ is normal because it emanates from a point (or object) at the trap. Since the radius of the sphere, R, is arbitrary, we can define an angular intensity distribution for light wave entering or leaving the focus, $I(\theta,\phi)\hat{\mathbf{r}}d\gamma = \vec{\mathbf{S}}dA$, where θ and ϕ are angles shown in Fig. 2, $\hat{\mathbf{r}}$ is a unit vector from the focus, and $d\gamma = dA/R^2 = d\theta\sin\theta d\phi$ is an element of solid angle.

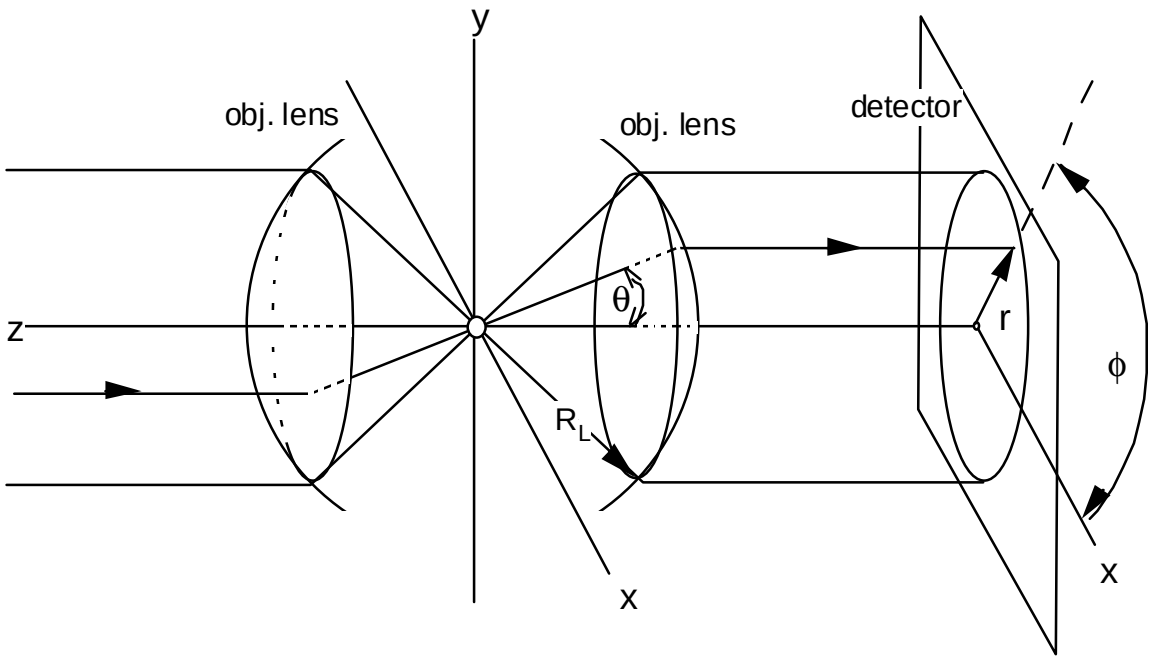

Figure 2. *Coordinate system for optical trap. Light enters from left and is focused to a spot where trapped bead is shown. A second lens, of focal length R, converts the exiting light to a parallel beam, which then falls on a photodetctor.*

Although it is difficult to *predict I(θ,ϕ)* for light scattered from an arbitrary object trapped at a focus, it is not difficult to measure *I(θ,ϕ)*. Once this task is accomplished, the force exerted by light on the object can be computed as

$$\vec{\mathbf{F}} = \left(n_l / 4\pi c\right) \iint I(\theta,\phi)\left(\hat{\mathbf{i}}\sin\theta\cos\phi + \hat{\mathbf{j}}\sin\theta\sin\phi + \hat{\mathbf{k}}\cos\theta\right) d\gamma \qquad (4)$$

Here $I(\theta,\phi)$ is a radiant intensity, measured in watts/steradian, which is considered negative for rays entering the trap and positive for rays leaving it. If the trap is empty (no particle there to deflect the rays) then $I(\theta,\phi) = -I(-\theta,-\phi)$ and the integral over all angles equals zero.

A convenient way to measure $I(\theta,\phi)$ is afforded by a version of the Abbe sine condition [22] which states that any ray emanating from the principal focus of a coma-free objective lens, inclined at an angle θ to the optic axis but still hitting the lens, will exit the image-side principal plane of that lens at a radial distance r from the optic axis given by

$$r = R_L\, n_l \sin\theta_l \qquad (5).$$

Here n_l is the refractive index of the liquid on the object side of the lens and R_L is an effective radius for the lens equal to its focal length. Although Fig. 2 fails to show the coverslip and air interfaces, which typically intervene along the path from focus to lens, the quantity $n_l \sin\theta_l = n_{Glass}\sin\theta_{\text{Glass}} = n_{Air}\sin\theta_{\text{Air}}$ is invariant (by Snell's law) for a ray traversing such flat boundaries so that Eq. (5) holds true regardless of such changes in media.

If the rays exiting the trap in a small element of solid angle $d\gamma/4\pi$ are projected without loss onto an area element $dA' (= r\, d\phi\, dr)$ on the image-side principal plane of the lens, then, by energy conservation, the irradiance E (in watts/m^2) on dA' is given by $E(r,\phi)dA' = \mathrm{I}(\theta,\phi)d\gamma / 4\pi$. If the lenses intercept all the light exiting the trap, then the expression for the force can be written as:

$$\vec{\mathbf{F}} = \frac{1}{c}\iint E(r,\phi)\left(\hat{\mathbf{i}}\frac{r}{R_L}\cos\phi + \hat{\mathbf{j}}\frac{r}{R_L}\sin\phi + \hat{\mathbf{k}}\sqrt{n_l^2 - \frac{r^2}{R_L^2}}\right) r\,d\phi\,dr \qquad (6)$$

where the integral is now taken over the surface of the image-side principal planes of the objectives.

The transverse ($\hat{\mathbf{i}}$ and $\hat{\mathbf{j}}$) components of the force can be integrated by placing position-sensitive photo detectors at those principal planes. A dual-axis detector of that type gives two difference signals, D_x and D_y, each proportional to the silicon detector's responsivity Ψ, and to the sum of local irradiances $E(x,y)$ weighted by their relative distances x/R_D or y/R_D from the detector center, where R_D is the detector's half-width. The light position signals are given by the following expressions:

$$D_x = \Psi \iint E(x,y)(x / R_D)dA' = \Psi \iint E(r,\phi)(r\cos\phi / R_D)dA'$$

$$D_y = \Psi \iint E(x,y)(y / R_D)dA' = \Psi \iint E(r,\phi)(r\sin\phi / R_D)dA' \qquad (7)$$

where the integrals are over the surface of the detector. By combining Eqs. 6 and 7, expressions for the two components of force transverse to the optic axis, F_x and F_y can be obtained in terms of the detector signals and known constants.

$$F_x = \frac{D_x R_D}{c\Psi R_L} \qquad F_y = \frac{D_y R_D}{c\Psi R_L} \qquad (8)$$

Instrument Design

Although several authors have used the deflection of the trapping laser beam to infer bead position, or empirically calibrate a test force [23, 24], it has not been possible to collect and analyze all of the light leaving a single-beam laser trap to determine its rate of momentum change. The measurement scheme depicted in Fig. 1 cannot actually be used in a single-beam trap because such a narrow cone of light (as depicted in the figure) will not efficiently trap an object. The scattering force due to reflected light would overcome the axial gradient (trapping) force and the object would escape toward the right. But if a high-NA beam were used instead, then the analysis lens shown in Fig. 1 could not collect the marginal-exiting rays. After interacting with the bead (subjected to an external force), marginal rays in a single-beam trap would be deflected further off axis and fall outside the NA of the collection lens. To avoid this dilemma, a counter-propagating dual-beam laser trap was constructed similar to those of Buican [25]. Here, use of low-NA beams inside high-NA objectives allows significant beam deflection while still collecting nearly all the light. Each objective is used twice, focusing one beam while collecting the other beam for analysis. The two beams are directed to different detectors by polarizing beam-splitters as shown in Fig. 3. Use of quarter-wave plates before the objective lenses ensures that light reflected from the particle is not returned to the lasers but instead is reflected back to photo detectors, where its momentum change is registered properly.

A position-sensitive photo detector can be thought of as a large-area PIN junction photo diode bonded to a planar resistor. A light ray falling onto the detector surface produces a localized electric current proportional to the ray's power. That current is injected into the resistor surface so that the signal is proportionately divided between the output resistor terminals, depending on the initial location of the ray. The difference between the two output currents is a signal representing the sum of the powers of all rays, weighted by their distance from the detector center, as per Eq. (7). A dual-axis detector (e.g. United Detector Technology DL-10) has one planar photo diode sandwiched between two orthogonal planar resistors (see Fig. 4) so it outputs both x and y position signals. Such photo detectors cannot be placed at the output principal planes, which lie inside the objectives, so relay lenses ("L1" in Fig. 5) were used to re-image the principal planes onto the photo-detectors. The detectors measure only the light exiting the trap, not entering it, so they perform only half of the integration required in Eq. (4). This problem is solved by aligning the detectors on the optic axis so that, when no bead is present in the

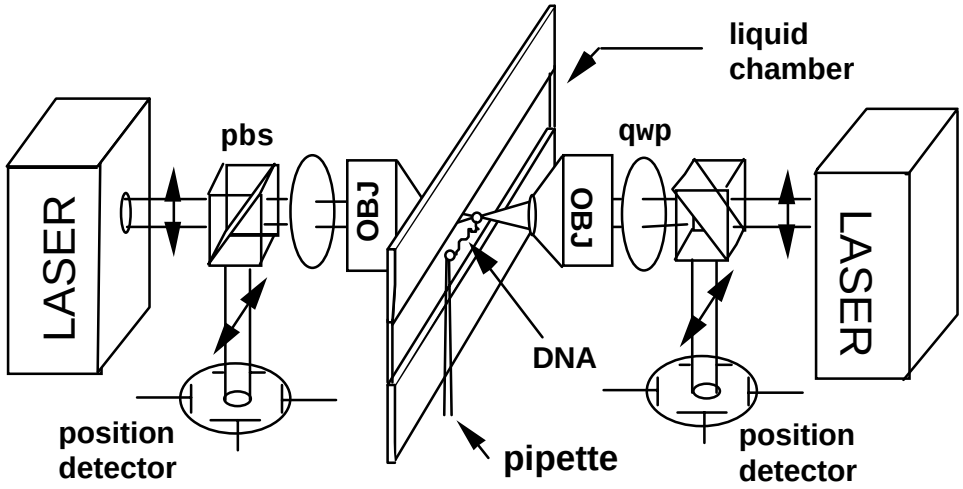

Figure 3. *Two diode-laser beams with vertical linear polarization pass through polarizing beam splitters (pbs), quarter-wave plates (qwp) and microscope objective lenses (OBJ). A bead is trapped at their common foci in circular polarized light. The exiting beams are collected by the opposite objective, converted to horizontal-polarized light and directed to position-sensitive photo detectors. The flow chamber is 2 coverslips selected for flatness, spaced 200 μm apart by parafilm layers and sealed by heat. The pipette is drawn from 100 μm glass tubing down to a point with an opening of ~0.5 μm.*

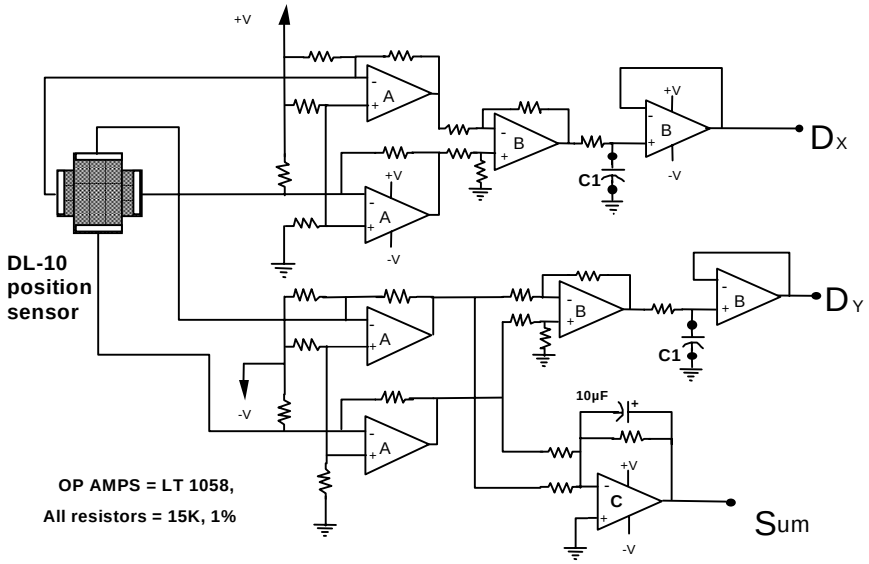

Figure 4. *Preamplifier to derive sum and difference signals from UDT DL10 position-sensitive detector. Current flows into the bottom layer of the detector (from upper op-amps), and out of the top layer (into lower op-amps). Capacitors C1 are chosen just large enough to average signal between data collection times, as set by the data acquisition system (not shown). Noise data were taken with capacitors removed. Then the rise time for a short laser pulse is ~10 μs, implying a bandwidth of ~100 kHz.*

trap, the output beams are centered on the detectors and the difference signals vanish, corresponding to zero volts at outputs "*Dx*" and "*Dy*" in Fig. 4. The light entering the trap carries no transverse momentum in this frame of reference and need not be considered even after a particle has been introduced. Only the exiting light is affected by interaction with the particle.

In practice, alignment of the two laser beams must be corrected as the room temperature changes. If the two beam foci are coincident and a bead is introduced into the trap with no external force acting on it, then each detector registers zero change in the transverse force. If the two beams are offset however, then one light beam pushes or pulls on the other light beam through their common interaction with the bead, and opposing force signals are registered at the two detectors. This difference signal can be used as feedback to correct misalignment by moving the x-y-z translator connected to the right objective shown in Fig. 5. The external force signal, which is the sum of the two detector signals, remains zero despite alignment errors. If an external force (e.g. a tethered molecule or viscous drag) acts on the bead, the two detector signals act in concert, and their sum gives the force according to Eq. (8). System calibration is independent of laser power because the detectors measure the light power themselves; the signals *Dx* and *Dy* (Fig. 4) are proportional to the product of beam offset and power. Transmission losses in the objective lenses and associated optics are incorporated into an effective sensitivity Ψ for the detectors.

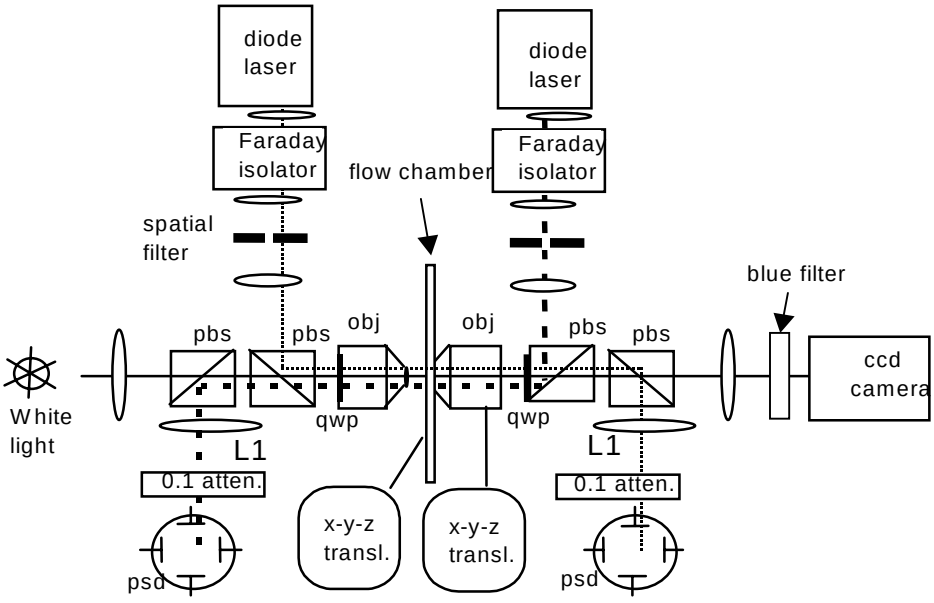

Figure 5. *Optical set-up. Diode lasers (SDL 5431, 835 nm, 200 mW) are mounted in temperature controlled mounts (Newport 700-C), beam-circularized with anamorphic prisms (not shown) and protected from reflections by Faraday-effect optoisolators (OFR IO5-835-LP). A spatial filter, (two 100 mm lenses, 40 µm pinhole) passes ~80% of the laser power. Polarizing beamsplitters, (pbs) (Melles Griot 03-PBS-064) separate different polarizations for infrared beams but pass blue light in either polarization for ccd camera image. Quarter wave plates (qwp) (CVI QWPO-838-05-4) for circularly polarized beam at foci. Objectives are Nikon 60X plan-Apo-water NA 1.2 with correction collars.*

Momentum-Flux Calibration

The light momentum-flux force transducer is calibrated from first principles, i.e. conservation of light momentum, without use of test forces such as viscous drag or thermal motion. Approximate values for R_L, R_D, and Ψ in Eq. (8) can be obtained from manufacturers specifications but it is best to measure these quantities *in-situ* to account for attenuation in lenses, cubes or filters and also the magnification factor from lenses L1 acting on the position detectors. To find R_L, a test stand was constructed where the objective was held fixed while a pencil of light was directed backwards through it (Fig. 6). The beam was offset various distances ΔX while the output angle θ was measured. A value for R_L was obtained by fitting the ΔX vs. θ data to Eq. (5). To find the effective detector radius, R_D, the objectives were removed and a movable source of parallel light (laser beam) was inserted in their place, as shown in Fig. 7. This beam was offset a variable distance ΔX as the voltage output Dx of the detector preamplifier (Fig. 4) was recorded. These data were fit to the function $Dx = Sum\ (\Delta X / R_D)$ where *Sum* is the total detector current (Fig. 4) and R_D is chosen for best fit. The effective detector sensitivity, Ψ relates the detector output current ("*Sum*") to the light intensity *at the trap focus*. Therefore the attenuation from one objective must be included, as well that of the chamber, cubes, attenuators and lenses. To measure Ψ a flow chamber was fitted as shown in Fig. 3, the objective foci were made coincident, but then only one laser was operated at a time. The power from this laser was monitored upstream and downstream from the pair of objectives using a Newport 840/818-ST meter. Then the power at the focus was estimated as the geometric mean of those two readings and Ψ was calculated as the detector output ("*Sum*") divided by the power at the focus.

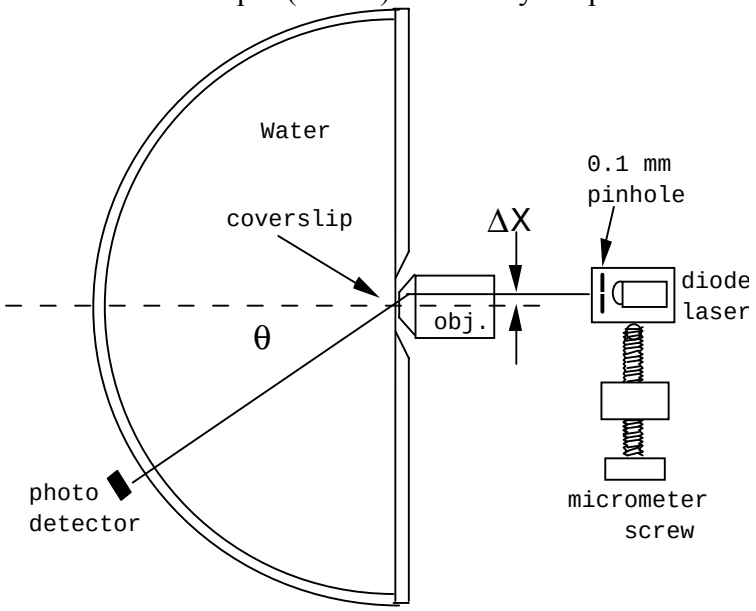

Figure 6. *Objective lens test jig with a diode laser (Melles-Griot 560LB108, 830 nm, 30 mW) carried on a translation stage. A semi-circular trough of water is constructed of Plexiglas with a glass coverslip window. A split photodiode UDT SPOT-9 detects the output beam angle.*

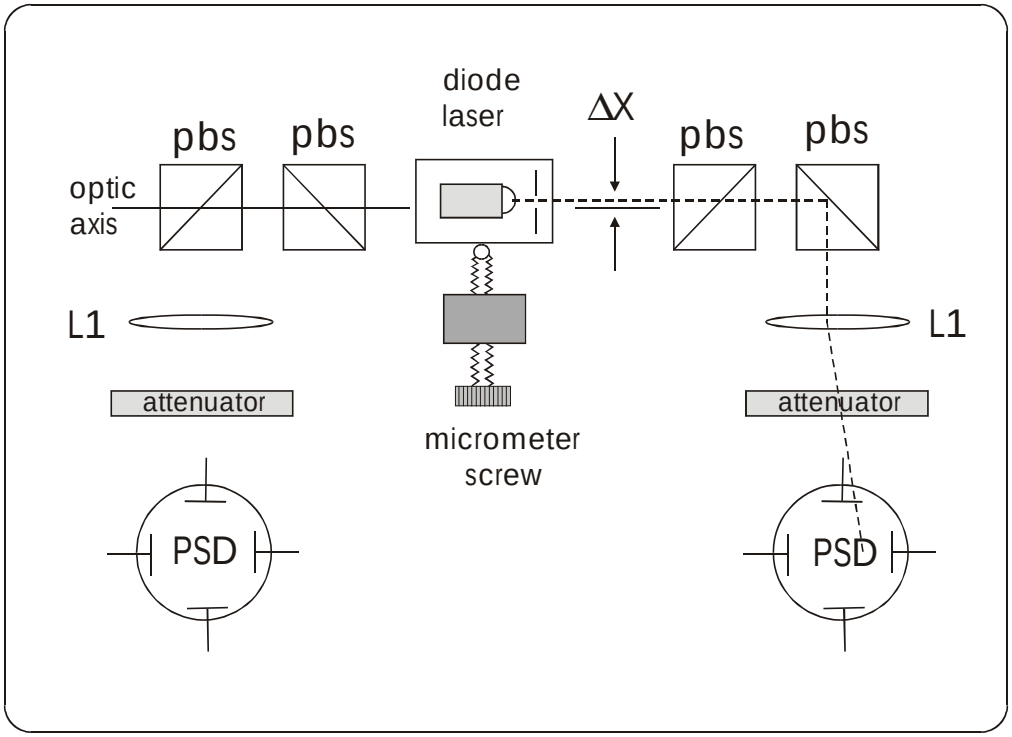

Figure 7. *Device to test for effective radius (R_D) of photodetector. The objective lenses are removed from the trap set-up and a test laser (830 nm, 30 mW with 100 μm pinhole) simulates light from an objective. The beam is translated a distance ΔX while the differential current from the position-sensitive detector is monitored.*

To test the range of applicability of Eq. (5), seven objectives lenses were the tested in the apparatus of Fig. 6.

1. Nikon E, 40X air, NA=0.6
2. Nikon E-plan 40X air, NA=0.65
3. Nikon CF plan-Achromat 60X air w/corr., NA=0.85
4. Nikon plan-Apo 60X water w/corr., NA=1.20
5. Zeiss plan-Neofluar 63X oil, NA=1.25
6. Nikon 100X oil, NA=1.25
7. Zeiss plan-Neofluar 100X oil, NA=1.3

The input angles (θ) versus output offsets (ΔX) were tested at 15 to 20 positions across the lens and fitted to the function $\Delta X + m_1 = R_L\, n_l \sin(\theta + m_2)$ where R_L, m_1 and m_2 were adjusted for best fit. All 7 objectives matched Eq. (5) over their entire back-aperture width to within the measurement error, which was ±0.05% of an offset reading. A condenser lens was also tested, namely a large oil-immersion "Abbe" lens with NA =1.25 and 1 mm working distance. It had a detectable error of 0.5% at its greatest offset. For visible light (670 nm) it was found that R_L always equaled 160 mm divided by the nominal magnification of the lens, to within ±5%. The lens most often used in our tweezers, number 4 above, was tested again at 830 nm and found to have a slightly

shortened effective radius of 2.50 mm at that wavelength. Since this lens was designed for a conjugate focal distance (tube length) of 160 mm, it was convenient to convert it to an infinite conjugate focus by placing a -150 mm lens immediately behind it (not shown in Fig. 5). This extra lens had the effect of reducing R_L to 2.25 mm. Also, R_L varied by ± 2.5 % across the range of that objective's correction collar settings. Therefore it is best to calibrate an objective at the trap wavelength, with its negative lens in place (if used) and with fixed correction-collar position.

Force Sensor Test Results

When a particle is trapped at a focus, most of the trapping light is refracted and collected by an objective (as shown in Fig. 1) but some light is scattered outside the collection angle (NA) of the objectives. This effect registers as a drop in the total power received by the photo detectors when a bead is introduced into the trap. To measure the efficiency of light collection, polystyrene beads of 8 different sizes, ranging from 0.27 μm to 20 μm diameter, were introduced into the trap while the detector output ("*Sum*" in Fig. 4) was recorded. Table I lists the percentage of the light collected after introduction of a bead at the focus.

To test the effect of particle size on light-momentum force measurements, various-sized polystyrene beads were trapped and exposed to fluid flow while the light-force sensor output was compared with the drag force, as calculated by Stokes' law. Translating the fluid chamber back and forth past the laser focus should create a homogeneous flow field. The speed was varied by hand and monitored by an electronic micrometer attached to the chamber. Results over a range of speeds and bead sizes are plotted in Fig. 8. The vertical coordinate in Fig. 8 plots the light-momentum sensor output, converted to force by Eq. (8), where the constants R_L, R_D, and Ψ were calibrated as described above (Figs. 6 and 7). The points fall near a line with a slope of one, indicating agreement between the two methods. Individual best-fit slopes for 8 different bead sizes are entered in Table 1 under "Light/Stokes".

Another way to check calibration of the force sensor is to measure the thermal forces acting on a trapped bead and compare the measured values with the theory. The spectral density of displacement-noise for an overdamped particle in a harmonic potential is given by [26]

$$\left\langle \Delta x^2(\omega) \right\rangle_{eq} = \frac{2k_B T}{\xi\left(\omega_c^2 + \omega^2\right)} \tag{9}$$

where ξ is the damping constant (drag coefficient) for the bead moving in a viscous medium, κ is the spring constant, and $\omega_c = \kappa/\xi$ is the corner frequency. Since the force $F = \kappa \Delta x$ in the trap, the spectral density of force fluctuations is given by

$$\left\langle \Delta F^2(\omega) \right\rangle_{eq} = 2\xi k_B T \frac{\omega_c^{\,2}}{\left(\omega^2 + \omega_c^{\,2}\right)} \tag{10}.$$

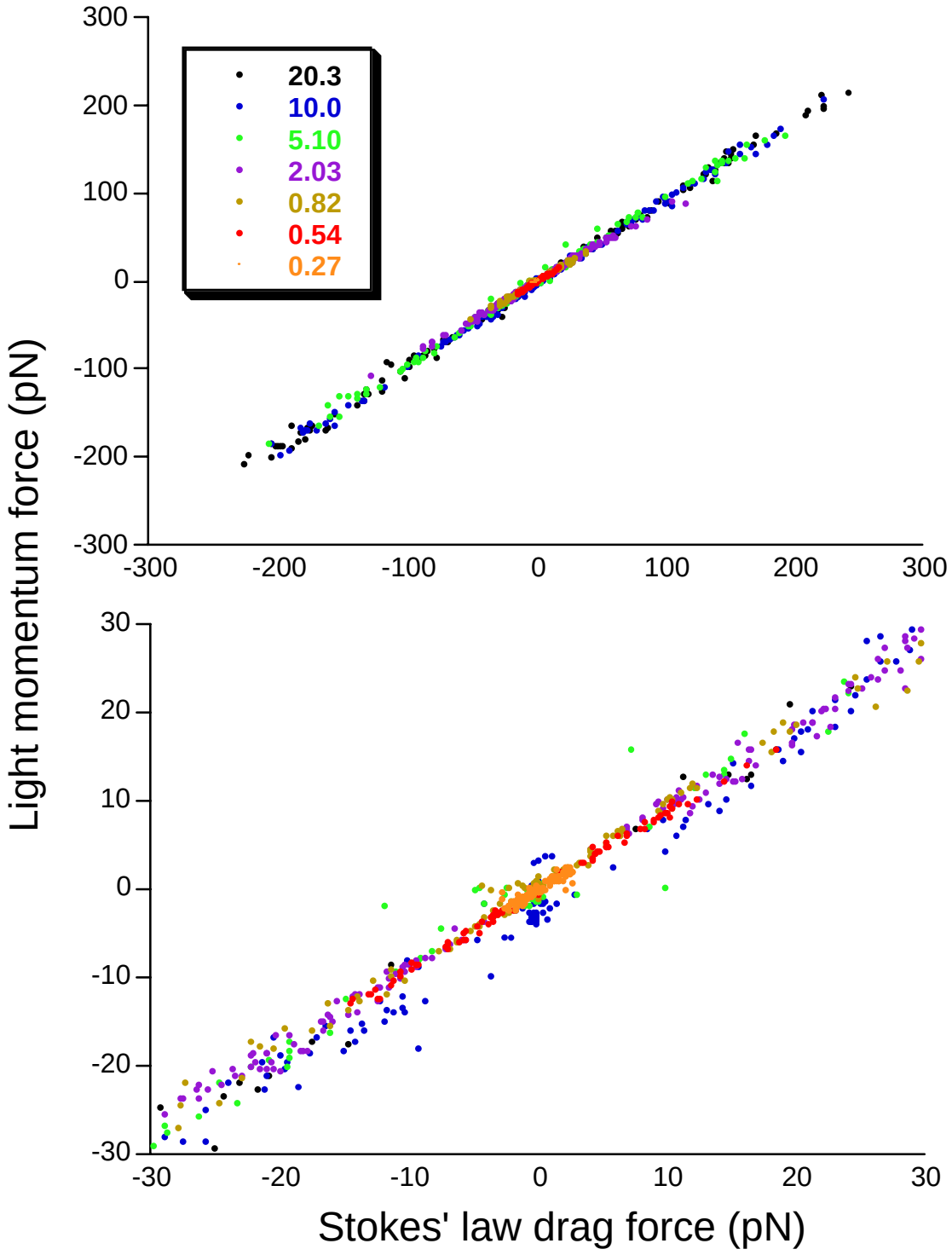

Figure 8. *Estimated viscous drag forces on 8 different diameter polystyrene beads are compared to light-momentum sensor output, calibrated using light momentum (Eq. 8). All beads were Bangs Laboratories Estapor size standards, except one bead by PolySciences which was reported as 1.05 uM in an earlier study [12], but resized using dynamic light scattering (Particle Sizing Systems, Santa Barbara, CA) as 0.82 μm in the present study. For the largest (20μm) beads, the walls of the fluid chamber were only 10 bead-radii distant, so Stokes' law was corrected by 12% to account for a 6% effect from both walls [8]. Bottom graph is 10x expansion of top graph, to show more small-bead data.*

Far below the corner frequency, the force-fluctuation spectral density is almost constant at a value given by

$$\left\langle \Delta F^2(\omega) \right\rangle_{eq} = 2\xi k_B T \qquad (11).$$

Above the corner frequency, force fluctuations decay rapidly as $1/\omega^2$.

To calibrate with thermal noise, we recorded the force fluctuations for trapped beads using a fast A/D converter and obtained power spectral density (PSD) distributions by Fourier transform of the data. To make plots with units of picoNewtons, the output from the preamplifier (in volts) was converted to force by using Eq. (8) with calibration factors obtained as per Figs. 6 and 7. If the light-momentum calibration is accurate, then the force PSDs should agree with theory and plateau at levels given by Eq. (11). Beads of five different sizes were tested and their PSDs are plotted in Fig. 9. Note the plateau levels (force-axis intercepts) increase with bead size since the drag coefficient, ξ, for the bead also scales with size. Knowing the bead radius, r, and substituting the Stokes'-law drag coefficient, $\xi = 6\pi r\eta$ (where η is the viscosity), permits direct comparison between the light-momentum sensor output and the thermal force. Results are listed in Table I under "Light/Thermal" where the plateau levels for the PSDs were averaged over the frequency interval between 100 Hz and 200 Hz, except for largest bead, where 25 Hz is used due to its low corner frequency.

The maximum transverse holding force of the trap was measured by trapping polystyrene beads of various sizes and increasing the flow of water through the flow chamber until they escaped. The light-momentum sensor, calibrated by Eq. (8), measured the drag force up to the point of escape. A trapping efficiency was then calculated as per Wright et al. , $F_{esc} = Q_{trans}\, n_l W_{trap}/c$. This efficiency is labeled Q_{trans} in Table I, since the bead always escaped in a direction transverse to the optic axis. For large beads (> 1 wavelength) the force sensor output becomes non-linear before F_{esc} is reached, as shown in Fig. 10, but smaller beads display linear output up to F_{esc}.

Table I *Effect of bead size on light-force calibration.*

Bead diameter μm	light collected %	Light/Stokes	Light/thermal	Q_{trans}
0.27	99.8	0.85	0.90	0.005
0.54	98	0.90	0.95	0.03
0.76	96	0.88	0.96	0.06
0.82	95	0.90	1.03	0.11
2.03	98	0.88	1.04	0.25
5.10	99	0.94	1.02	0.39
10.00	99.5	0.96	a	0.40
20.30	99.5	0.95	a	0.40

[a] *values not accessible because corner frequencies too low.*

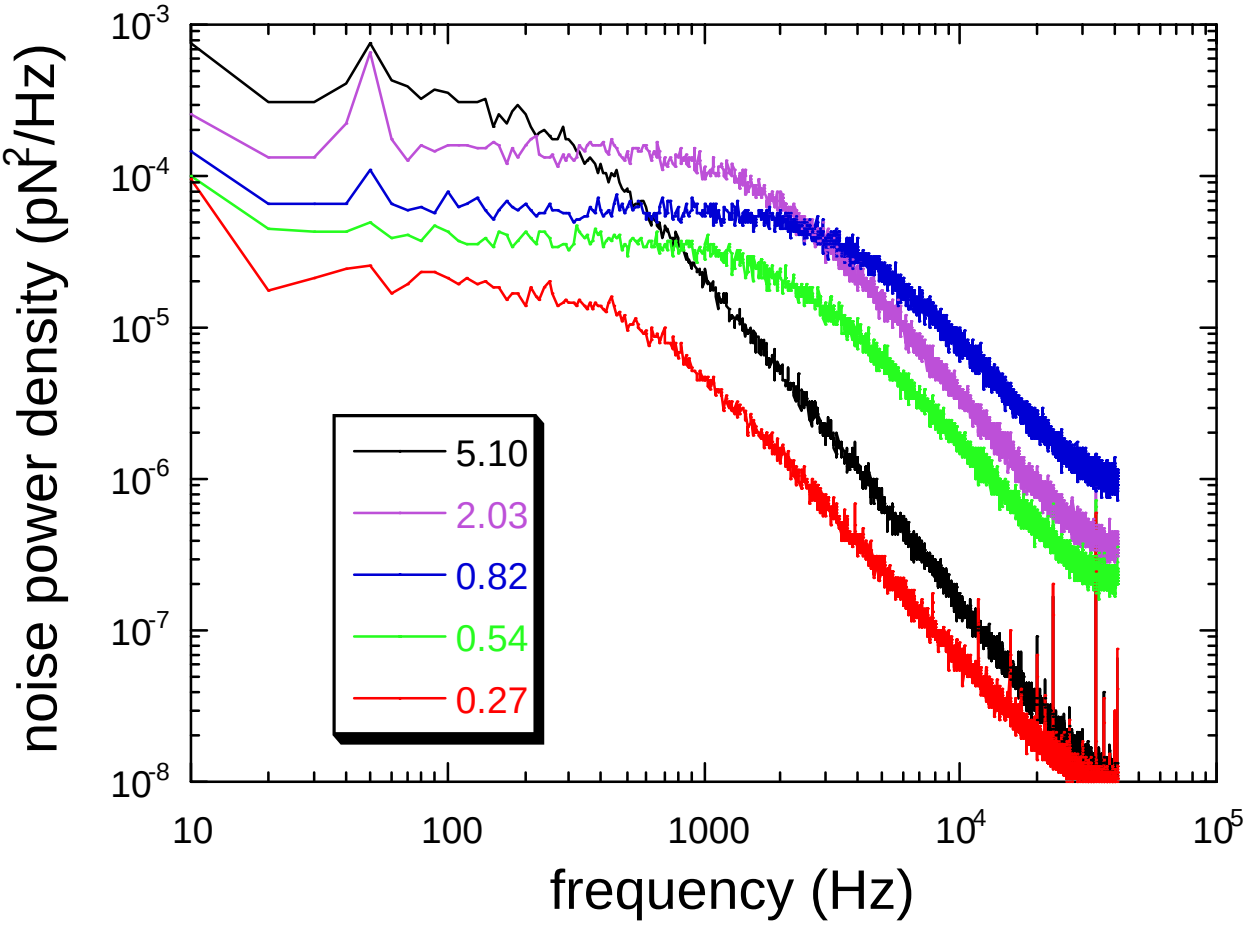

Figure 9. *Power spectral density distribution of force fluctuations from light-momentum force sensor using 5 different beads, sized 0.27, 0.54, 0.82, 2.0, and 5.1 μm in diameter. Five seconds of output was recorded at 100 kHz rate using a National Instruments PCI-MIO-16XE-10 analog-to-digital converter with 16 bit accuracy. Data were converted to a frequency domain with a discrete FFT (Igor Pro Ver. 3, Wavemetrics)*

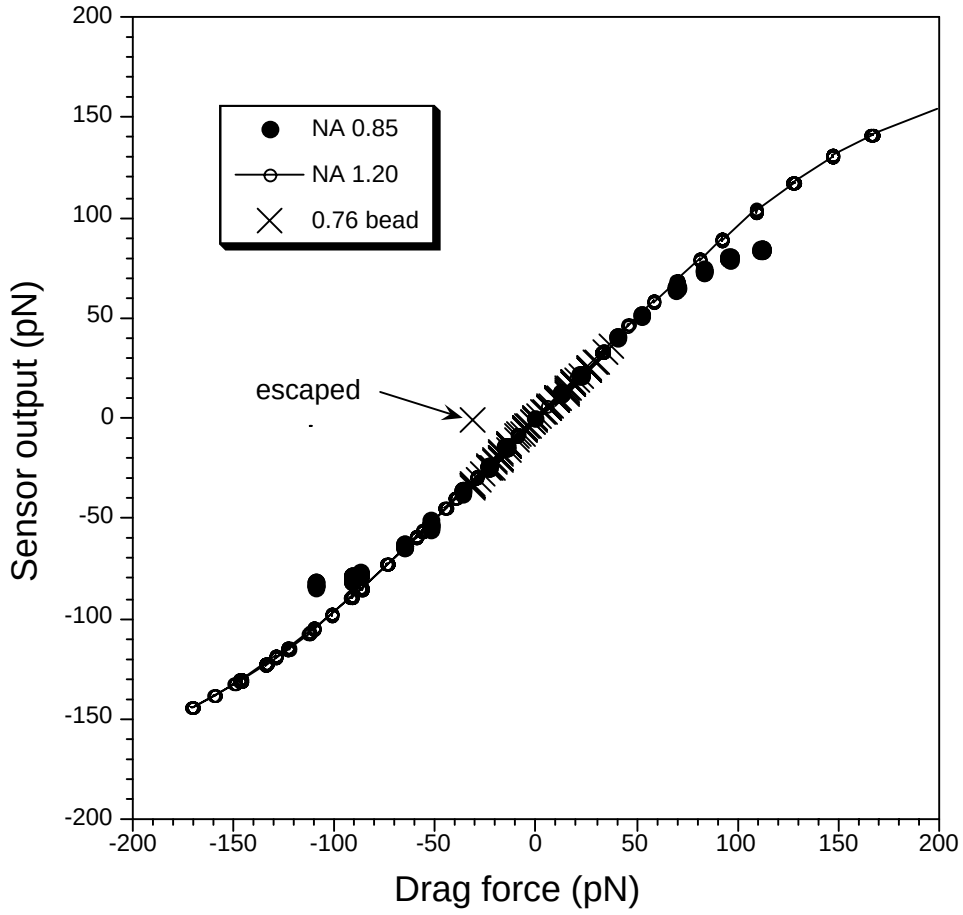

Figure 10. *Response of light-momentum sensor for beads that were pushed by fluid drag to the point of escape. Beads (2 μm diameter) were tested in two different trap set-ups, one with 0.85 NA objective lenses and 100 mW power, and the other with 1.20 NA lenses and 140 mW power. A smaller bead (dia. = 0.76 μm) was also tested in the trap with NA = 1.2 lenses.*

Finally, a different type of test force was used to determine the effect of various factors on light-sensor accuracy. When a dsDNA molecule is pulled above a certain force (65 - 70 pN) it undergoes a cooperative structural transition to a longer form [28, 29]. Since the force remains nearly constant during that transition, it can be used as a standard to test force transducer accuracy. Therefore, individual molecules of lambda-phage DNA were attached between the test bead and a pipette bead, as shown in Fig. 3, and extended in 500 mM NaCl buffer solution while the force sensor output was recorded. For a 7μm polystyrene test bead, the light sensor reported a force of "68 pN" at the midpoint of the stretch transition. The sensor output remained constant for a 4 μm and a 2μm test bead, as shown in Table II, but dropped to "64 pN" for a 1 μm test bead. Forces sufficient to cause DNA's structural transition could not be generated using beads smaller than 1 μm. The effect of laser power on sensor calibration was tested in a similar way. Here a test bead of 2μm diameter was pulled at DNA's transition force while the laser power was varied. Comparing the total laser beam power at the focus ("Power" in Table II) with the sensor output ("force") gave a nearly constant result over a 2:1 power range. Next, the effect of changing the shape of the trapped object was explored by placing several test beads in the trap at the same time. Multiple-beads align axially in a dual-beam trap and aggregate into chains. No change was seen in the transition-force reading when a single dsDNA molecule pulled a trap containing one, two or three beads (each 2 μm diameter). Finally adding sucrose to the 500 mM salt solution tested the effect of changing the refractive index of the buffer. In buffer containing only salt, the transition force output read "68 pN". Adding 20% sucrose (by weight) made the output drop to "67 pN" but increasing the sucrose to 33% restored the output somewhat to "67.5 pN". Here the refractive index was increased from 1.34 for salt buffer to 1.40 for high-sugar buffer, while the index for the polystyrene bead remained 1.57. Therefore the relative index (bead/buffer) decreased from 1.17 to 1.12 and the index change (bead minus buffer) dropped by ~30% without appreciable change in force calibration.

Table II *Effect of bead size and trap power on standard force measurement.*

Bead diameter	measured force	power (mW)	measured force (pN)
(μm)	(pN)	140[a]	68
7	68	120[a]	68
4	68	80[a]	68
2	68	60[a]	67.5
1	64	50[a]	65

[a] *Power calculated at trap from known objective transmissions. All power comparisons use same size (2 μm) bead.*

Force Sensor Discussion. The counter-propagating-beam optical trap described here analyzes the light-momentum flux leaving the vicinity of a trapped particle and reports the force that the flux has exerted on the particle. It is assumed that nearly all of the light leaving the trap is collected. As seen in Table I, this assumption seems justified since the measured collection efficiency for an objective with NA=1.2 was 95 to 99

percent. Little scattering is expected for large diameter (>>1λ) spherical beads with small displacements from the focus. Then, as sketched by Ashkin [4], the output beam will be a cone of similar divergence to the input cone but deviated from the axis as shown in Fig. 1. For particles much smaller than λ, the Gaussian waist at the focus bypasses the particle. Therefore the transmitted light is seen to increase for the two smallest beads in Table I. The worst collection efficiency (95%) occurs for beads about 1λ in diameter. There is currently no theory that successfully predicts the scattering pattern for such beads near a focus [3, 27]. When an objective with NA=0.85 is used, the collection efficiency drops to 90% for a 1 μm bead. Since this lens subtends only ~11% of all (4π) solid angle as seen from the focus, the 1 μm bead must still scatter over a fairly narrow forward angle.

As seen in Table I, light-force measurements made on various-sized beads exposed to fluid drag and Brownian forces agree rather well with Stokes'-law and thermal theory calibrations, but with slight systematic errors of two types. First, the average of all comparisons is low for the light-force sensor. This effect might result from errors in estimating R_L, R_D, and Ψ of Eq. (8), but then why does the light-force sensor agree better with thermal measurements than with drag force measurements? Alternately, the assumption of uniform velocity for all fluid in the chamber may be erroneous. Our beads are trapped far (100 μm) from any wall. If stage acceleration sets up inertial convection in our fluid cell (sloshing through the fluid ports), then it will register as a decrease in the relative flow past the bead. The Light/Thermal results, where the chamber was not moved, are higher overall by 5%, in accordance with the sloshing hypothesis. A second type of systematic error occurs for beads which are ~1 wavelength in diameter. They show an additional 5% force deficit from the light-force sensor. This error probably reflects the uncompensated loss of 5% of the trapping light, scattered outside the lens NA. In future work, it should be possible to measure the light loss and compensate this force error.

It might seem odd that light-sensor accuracy improves again as the particles become smaller than the trap wavelength (e.g. 0.27 μm, Table I), since the tiny amount of light interacting with the particle is scattered over an increasingly large range of angles. To understand this effect, suppose the trapped particle were reduced in size until it became a Rayleigh scatterer with a perfectly symmetrical (about its own center) radiation pattern such that the irradiance is proportional to $\cos\theta$ but omni-directional in ϕ. Of the light which was scattered by the particle, only ~60% would be collected by two objective lenses with NA = 1.2. Such loss seems to insure a force-measurement error. However, any transverse force on a trapped particle must be represented by a transverse asymmetry in the far-field scattered intensity pattern if momentum is conserved. Since the Rayleigh pattern itself is symmetric about ϕ, the requisite asymmetry must be caused by an interference between the Rayleigh waves (emanating from a source offset in the trap) and the spherical trap-beam waves emanating from the trap focus. Since the intense spherical waves are created by lenses and truncated to lie in a cone that is collected by those lenses, the asymmetrical interference pattern also lies within that cone, since there can be no interference where one set of waves (e.g. from the trap beam) is missing. The part of the Rayleigh pattern that misses the lenses is symmetrical and carries no net transverse

momentum. Given that the transducer works properly for bead diameters much larger than a wavelength (ray optics) and much smaller than a wavelength (Rayleigh regime), it is perhaps not surprising that it also works fairly well for beads diameters near one wavelength.

Analysis of the transverse (x and y) components of light momentum is based on the Abbe sine condition, Eq. (5). Probably all objectives meet this criterion with negligible error since little error (<0.05%) was detected in the seven objectives we tested, which ranged in price from $150 to $9,000. Three factors affect the choice of an objective. (1) It must have a long working distance to reach the middle of the fluid chamber. (2) Water immersion is preferable because the two foci remain coincident while the fluid chamber is translated sideways several millimeters. If the walls of the fluid chamber are not perfectly parallel, then variations in the chamber-water thickness cause beam misalignment for air-immersion lenses. Using water-immersion, however, the total water thickness inside and outside the chamber remains constant. (3) The lens NA should be large. Although a counter-propagating dual-beam trap uses narrow beams which under-fill the objectives, those beams deviate from the optic axis when an external force is applied to the trapped object (see Fig. 1). Extra aperture must be allowed for this deviation or light will be lost. If we call the radius of the trap beam r_{beam} and that of the back aperture of the objective r_{ba}, then the maximum distance the output beam can deviate before light signal is lost is the difference between these two radii r_{ba}-r_{beam}. This offset represents an angle θ given by $n_l \sin\theta = (r_{ba}-r_{beam})/R_L$. The force that produces such a deviation is given by

$$F_{max} = (W/c)\, n_l \sin\theta = (W/c)(r_{ba}-r_{beam})/R_L \qquad (12)$$

where F_{max} is a maximum force, above which the sensor loses accuracy. For instance, a Nikon CF plan-Achromat 60X-air lens was used with the following specifications: NA = 0.85, R_L = (160 mm/60X) = 2.667 mm and $r_{ba} = R_L$ x 0.85 = 2.267 mm. The laser beam diameter was measured where it entered the lens and found to be r_{beam} = 1.624 mm. By Eq. (12), F_{max} = 50 pN for W = 100 mW. As seen in Fig. 10, the output from this force sensor does become non-linear above 50 pN. When a 60X lens with NA = 1.2 was used instead, F_{max} increased to ~100 pN, as shown in Fig. 10.

Low values of Q_{trans} for bead diameters below 1 λ (see Table I) reflect a drop in the polarizability of small particles, proportional to the particle's volume. Rayleigh scattering arguments (above) suggest that force measurements remain accurate for any force, as long as the (small) particle remains trapped. Accordingly, Fig. 10 shows that a 0.76 μm bead escaped the trap without detectable non-linearity, since $F_{esc} < F_{max}$.

Measuring Extension

The primary use of optical tweezers in biology has been to make real-time measurements of force vs. molecular extension (or position). Thus, despite the fact that the light-momentum sensor allows us to infer the force on a particle without measuring

its position, it is still necessary to measure particle positions quickly and accurately. One method to measure bead position is video microscopy. Figure 11 shows the image of two beads, one held on a pipette by suction, the other held in a laser trap. Kohler illumination is set for parallel rays at the object to enhance contrast. A bright spot forms at each center because the beads act as lenses. We locate the centroid of these spots by capturing the image and operating on it with an algorithm ("fillNeighbors", Fig. 11) that fills the interior of the dark rings while averaging the pixel positions. Using a 60X magnification and a 1/3" CCD camera (Watec LCL-903HS), the pixel size in Fig. 11 is 150 nm. Pixel averaging refines this resolution by about 10 times, so that the RMS repeatability error ("jitter") between successive frames is 10 – 15 nm. Such jitter is evident in Figure 12, which shows the video-detected position of a 2 uM bead, stuck on the top of a pipette, which was moved up and down 100 nm by a piezo actuator.

```
procedure fillNeighbors(level:byte; x,y:integer; fillByte:byte);
var brightness:integer;
begin
brightness:=videoPixelLevel(x,y);
if (brightness>level) and (globSize<globMax)  then
   begin
   xSum:=xSum+(x);
   ySum:=ySum+(y);
   putVideoPixel(x,y,fillByte);
   inc(globSize);
   fillNeighbors(level,x+1,y,fillByte);
   fillNeighbors(level,x-1,y,fillByte);
   fillNeighbors(level,x,y+1,fillByte);
   fillNeighbors(level,x,y-1,fillByte);
end;
```

Figure 11. A: *Video image of 2 μm bead on pipette with 3 μm bead above in trap.* ***B:*** *Recursive procedure "fillNeighbors" calls itself but returns when all interior pixels have been converted to dark (fillByte) level. Variables xSum and ySum divided by globSize give pixel-averaged x and y coordinates of bead.*

Faster and finer position data can be recorded for the pipette bead by using a relatively inexpensive "light lever" device attached to the pipette stage (see Supplementary Data in [9]). Such device comprises a single-mode optical fiber coupled to a diode laser (Thorlabs LPF-3224-635-FC), a PSD as in Fig. 4, and a lens attached to the pipette/chamber frame (Thorlabs C140TM-B). This lens collimates light from the fiber and directs the output bean onto the PSD. Since the focal length of the lens is short (1.45 mm) but the distance to the PSD is large (610 mm), a tiny movement in the relative position of the fiber translates into a 420-fold greater movement of the light spot on the PSD. When the PSD is coupled to a 16-bit A/D converter with 10V input range (ComputerBoards PCI-DAS1602/16), the distance resolution becomes 1.5 nm. The light-lever's increased resolution over video microscopy is evident in Fig. 12. Now the

hysteresis of the piezo-actuator stage (Thorlabs MDT-631) becomes clearly evident.

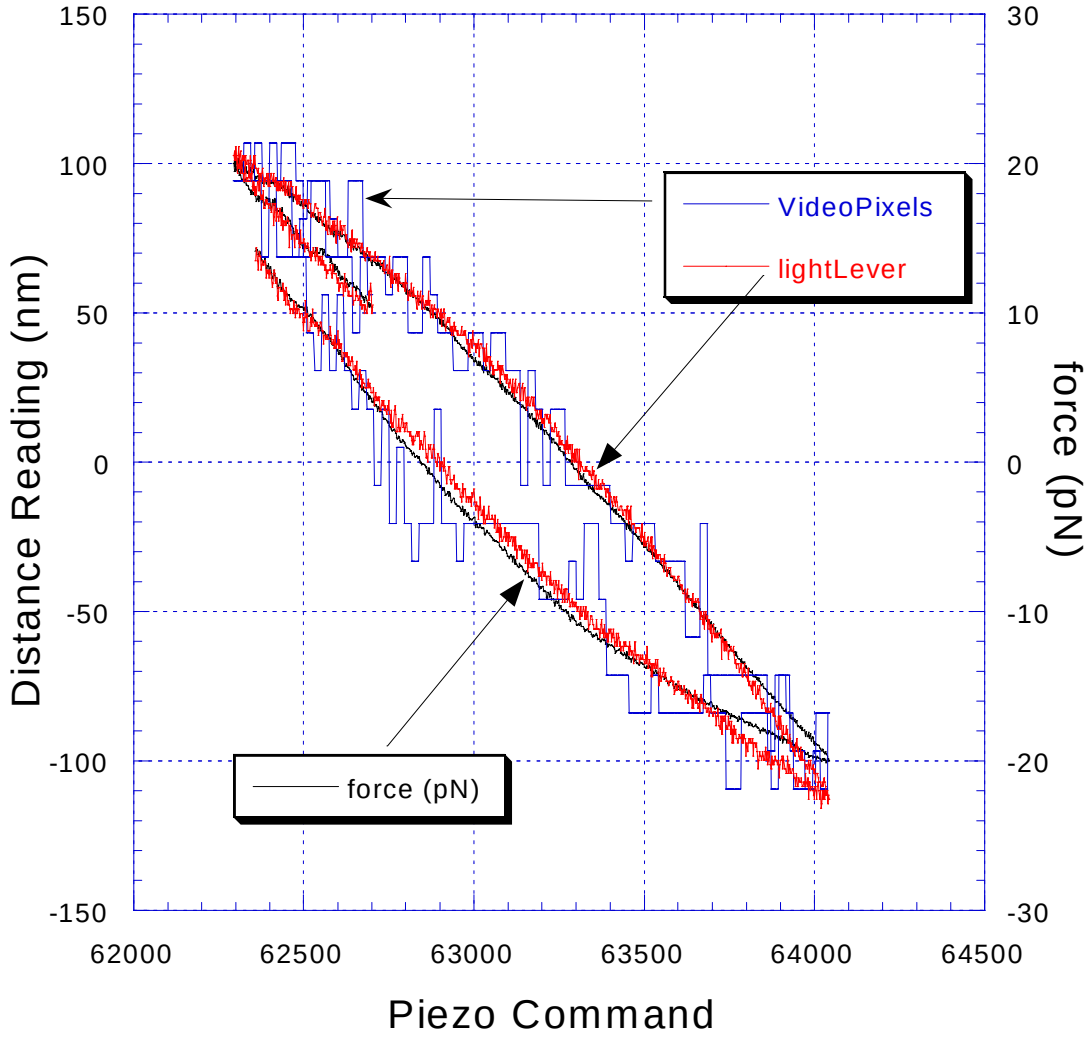

Figure 12. *Video-capture position (red) and lightLever position (blue) measured in nanometers (left scale). Light-force sensor output (black) in pico-Newtons (right scale). All outputs plotted versus piezoUnits i.e. positioner command from 16-bit A/D converter, open loop.*

For ultimate resolution, the bead in the optical trap can act as sort of a light lever itself [30]. Although the output of the light-force sensor records force, that force can be related to a movement of the bead in the trap by dividing force by trap stiffness. The problem then becomes one of estimating trap stiffness, since it varies with a number of factors (see above). Figure 12 also shows the fine resolution and low noise of this method. Note, however, the force-signal scale was arbitrarily normalized to give the same heights to the trap-force and light-lever traces. Different scale factors would be needed for different-sized beads or different laser powers.

Limiting Resolution

So what is the limit of spatial resolution for such a force-to-distance conversion? The single-bit resolution of the force detector circuit (0.016 pN), along with typical trap stiffness (~170 pN / μm for a 2 μm bead), suggests a limiting resolution of 0.1 nm. However the actual resolution is limited by position noise between the pipette and the trap position, and the system bandwidth. To characterize such noise, the pipette was directly attached to the bead in the optical trap. That bead was then moved up and down by ~1 nm using a piezo actuator stage. Bead position was monitored with both the light-lever and the light-force sensor at a sampling frequency of 200 Hz. Figure 13 shows such data time-averaged down to a bandwidth of 20 Hz. Here, position noise appears to exist mainly in separate time domains: slow drifts with >10 s duration, and fast vibrations with <0.05 s period. Its presence correlates with external factors such as room temperature change (slow), floor vibrations (fast), low-pitched voices (fast), fan motor noise (fast), dust crossing laser beams (slow), and general air currents. Our instrument was on an air-supported table. To obtain Figure 13, we worked silently on a quiet weekend in a sub-basement lab with room ventilation blocked. We allowed one hour (thermal) settling time after touching metal parts on the light lever or piezo stages with our hands. Some vibration noise in Fig. 13 could have been prevented, since a Fourier transform of the force-sensor noise (Fig. 14) shows a peak at 51 Hz. due to acoustic noise from a (barely audible) fan motor on a nearby computer. The general rise in the spectrum at 100 Hz is due to room acoustic noise exciting a mechanical resonance of the pipette's piezo stage.

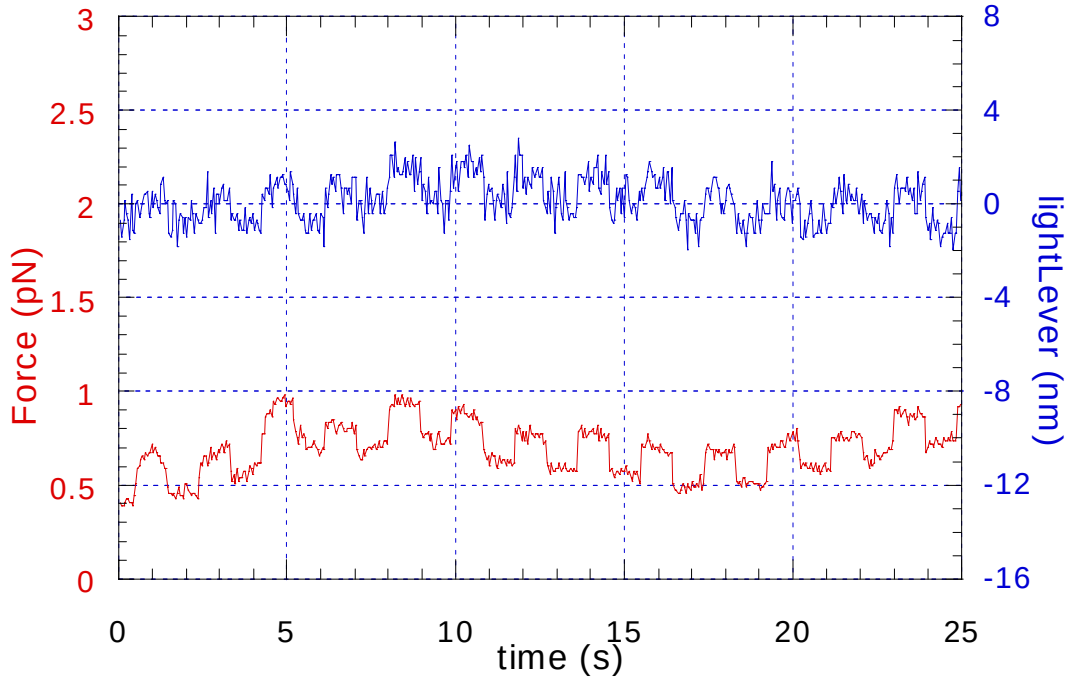

Figure 13. *Light-force sensor output for 2 uM bead in trap, which is also sucked onto pipette. Pipette moved with step size of 10 piezoUnits = 1.3 nm. Upper trace is lightLever, lower is light-force sensor.*

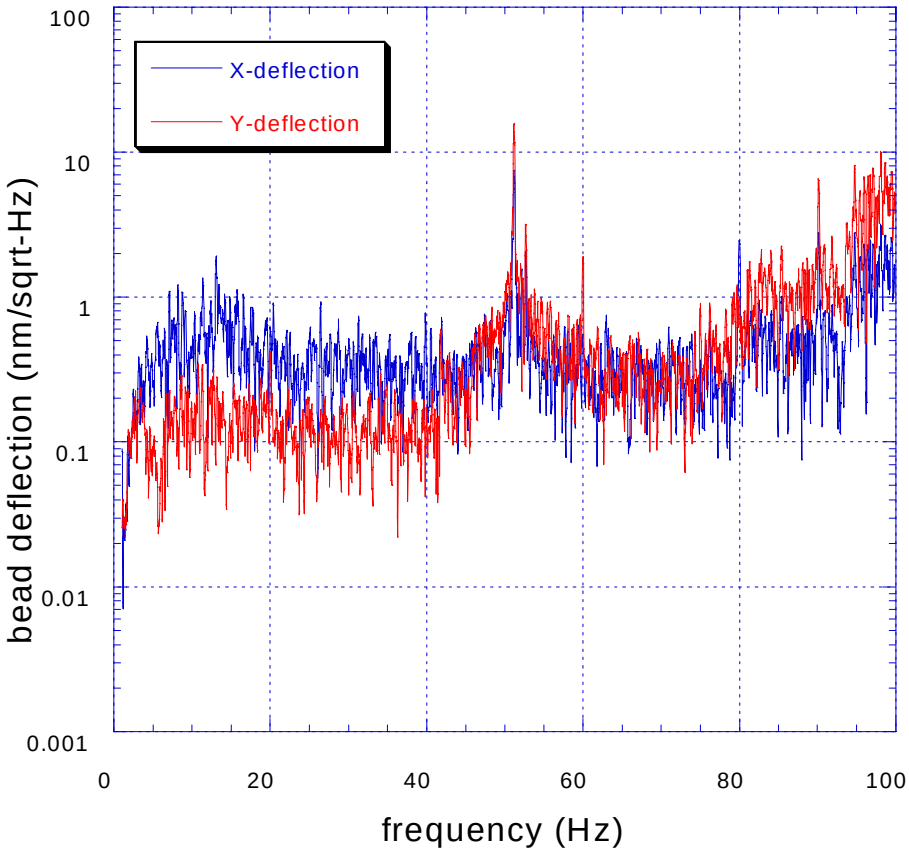

Figure 14. *Displacement-noise spectrum of pipette bead placed in optical trap inferred from light-force signal with assumed trap stiffness of 1e-4 N/m. X-axis noise spectrum in blue, y-axis noise in red.*

A real molecular experiment, however, usually involves a flexible coupling between the trap and the enzyme motor, such as a tether of DNA. Then thermal forces may set the limiting resolution of the experiment. The tether is elastic, so the bead undergoes Brownian motion in the trap, independent of any enzyme motor activity. To estimate such thermal motion, we integrate the noise power, Eq. (9), from $\omega = 0$ out to some bandwidth $B << \omega_c$ and get a value for noise displacement (Δx_{noise}) of a particle in a potential well.

$$\langle \Delta x^2 \rangle_{noise} = (2k_BT/\kappa)\,(B/\omega_c) = 2\,k_BT\,B\xi/\kappa^2 \qquad [13]$$

where κ is the stiffness of a trapping potential. But κ for the bead is not due to the optical trap alone, but the sum of the trap and tether stiffness, since they act as two springs in parallel: $\kappa = \kappa_{trap} + \kappa_{tether}$. Thus the RMS distance noise for a trapped bead with tether is

$$\langle \Delta x \rangle_{noise} = (2\,k_BT\,\xi\,B)^{1/2}/(\kappa_{trap} + \kappa_{tether}) \qquad [14]$$

Unlike the noise, the signal of interest, e.g. Δx_{step} of an enzyme motor, is reduced by using a tether with low stiffness. As pointed out by Yin et al.[7], this signal is divided

between two virtual springs in series, κ_{trap} and κ_{tether} and thus attenuated at the trap where it produces a signal given by

$$\Delta x_{signal} = \Delta x_{step}\ \kappa_{tether} / (\kappa_{trap} + \kappa_{tether}) \qquad [15]$$

To detect steps at the trap, the signal to noise ratio should be greater than one. Therefore Eqs. (14) and (15) give

$$\Delta x_{step} > (2\ k_B T\ \xi_{bead}\ B)^{1/2} / \kappa_{tether} \qquad [16]$$

Interestingly, the optical-trap stiffness does not affect limiting resolution [3, 31]. Drag coefficients are fairly important. Thus smaller beads are better than big beads because they have smaller drag coefficients. To the extent that this analysis may apply, an AFM cantilever should behave poorly because it has high drag. But the most important factor by far is the tether stiffness, as affected by average tether tension.

Tether stiffness rises rapidly with tension due to the non-linear entropic (bending) elasticity of a worm-like chain (WLC) with fixed contour length, roughly $F = (k_B T/4P)\ [(1-x/L)^{-2} - 1 + 4x/L]$, where x is the end-to-end extension of the chain, P is its persistence and L its contour length [32]. However, contour length is not strictly fixed, but increases with tension as $L = L_0\ (1 + F/S)$ where L_0 is the length at zero force and S is the enthalpic stretch modulus of DNA. Values of $\kappa_{tether} = dF/dx$ for the stretchable WLC using an improved power-series approximation [33] are given in Table III.

TABLE III. *Calculated tether stiffnesses for 10kb tethers of ssDNA and dsDNA under different tensions.* [a]

Tension F (pN)	1	2	5	10	20	50
κ_{tether} dsDNA (pN/μm)	4	12	42	98	170	250
κ_{tether} ssDNA (pN/μm)	1.3	1.5	2.6	7.2	20	74

[a] *Calculation assumes P_{ds}= 50 nm , P_{ss}=0.7 nm, $L_{o,ds}$ = 3.4 μm , $L_{o,ss}$ = 7 μm, S_{ds}=1000 pN, S_{ss} = 800 pN. Stiffness scales as 1/L for different length tethers.*

To test these predictions, we attempted to detect nanometer-sized steps through an 8 kbp tether of dsDNA. Figure 15 shows results where the pipette bead was moved up and down by 2½ nm while a trap bead registered changes in the force transmitted to it by the tether. Compare the force traces when the average tether tensions were set at 2 and 20 pN. The signal is transmitted clearly through tether under 20 pN average tension, but is barely discernable under 2 pN average tension. Indeed Eq. 16 and Table III predict that such a dsDNA tether, under 2 pN tension, requires a minimum step size of 2.6 nm to register above thermal noise in a bandwidth of 1 Hz i.e., the frequency of our signal (here B = 2π radians/s in Eq.16).

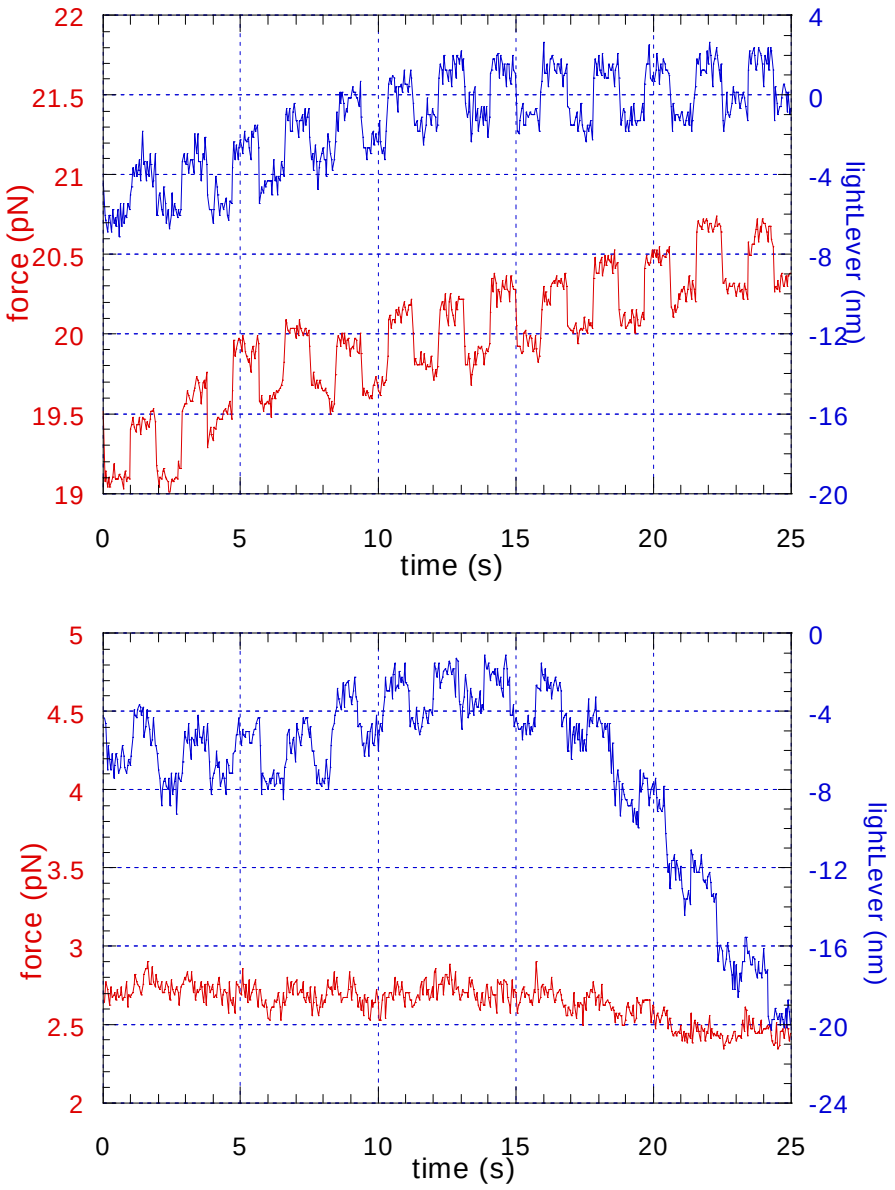

Figure 15 A: *Transmission of distance steps through 8 kbp piece of dsDNA, in 100 mM NaCl buffer, at high (~20 pN) molecular tension,* ***B****: same steps at low (~2.5 pN) tension. Upper traces are light lever output, lower are light-force sensor. Piezo Stage (Thorlabs MDT-631) moves pipette by 2.5 nm once every second. Trap bead diameter = 2 μm. Plot bandwidth = 20 Hz.*

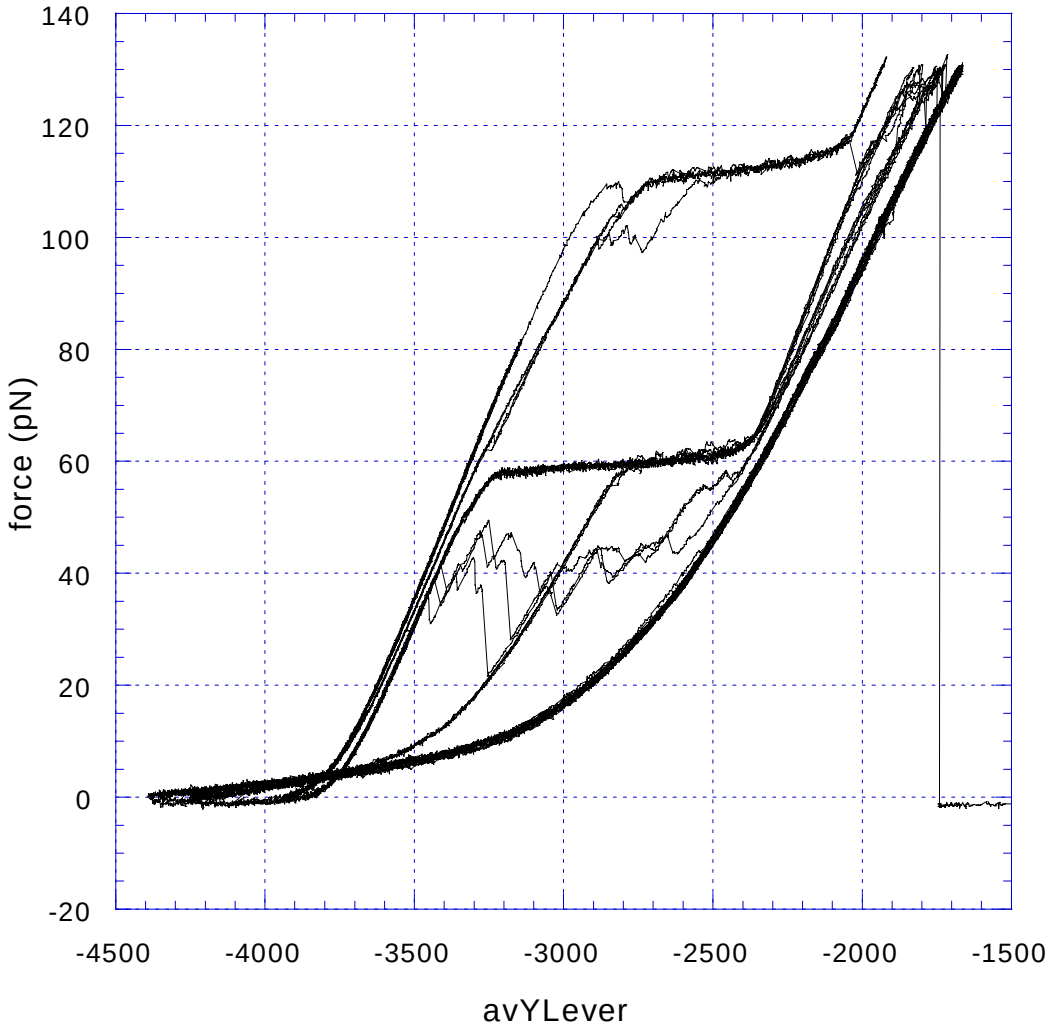

Figure 16. *Seventeen stretch/relax cycles of a 5 kbp section of plasmid pBACgusx11 (Novagen) pulled in 50 mM NaCl, 1 mM EDTA, 40 mM tris pH 7.5. One strand melts off repeatedly but remains attached at an end. It often starts to re-anneal when the force drops below 50 pN.*

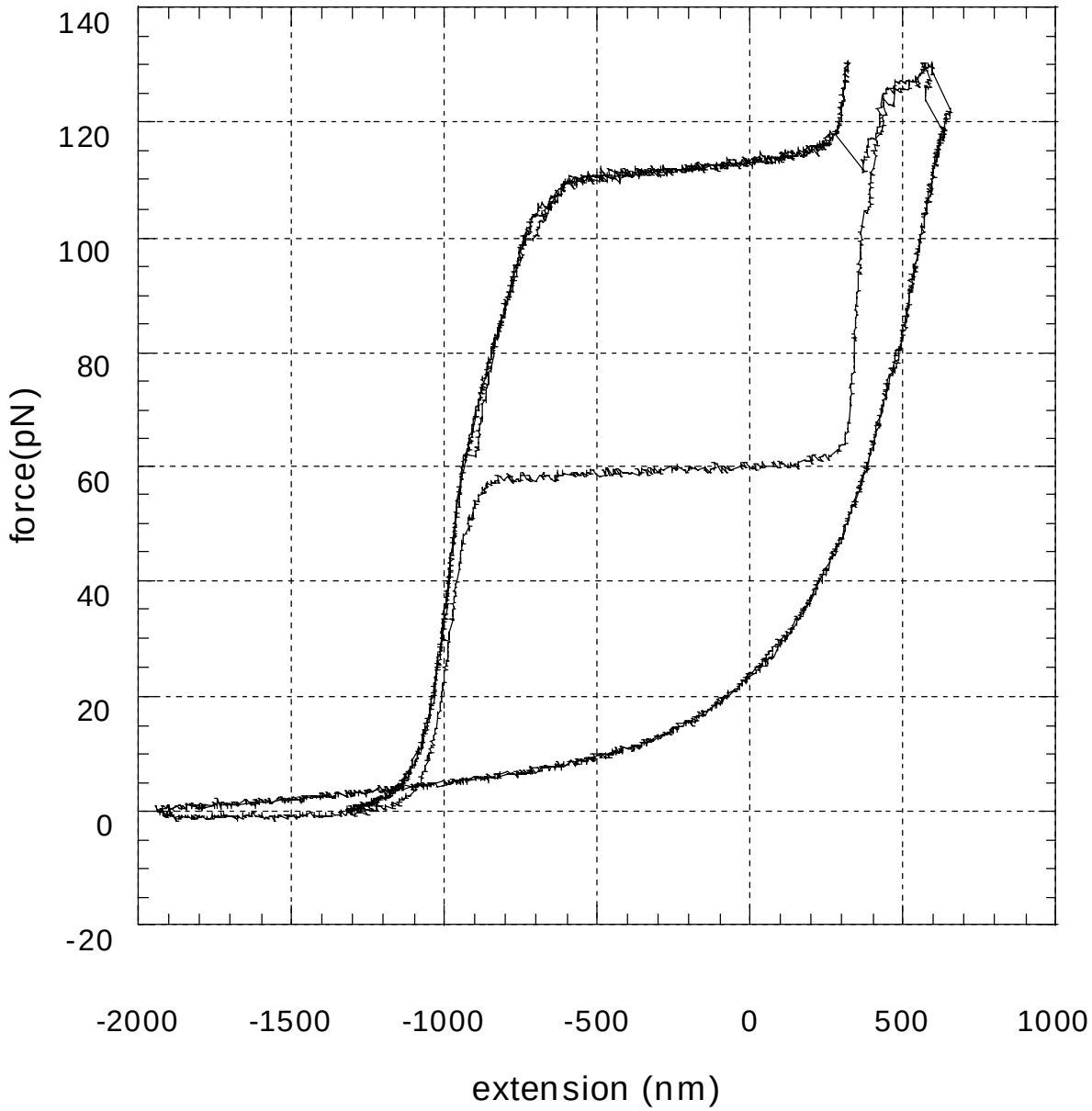

Figure 17: *First three stretch/relax cycles from previous figure, corrected for trap compliance. First cycle is reversible, staying on top curve for stretch and relax. Plateau at 110 pN indicates transition of torsionally constrained molecule to composite S-P form [34]. Second pull cycle follows upper curve, but single nick occurs at 115 pN, when it jumps to longer S-form. Plateau at 60 pN indicates B-S transition [28,29]. Further stretching causes S-form to melt at 130 pN [16, 35]. Bottom relaxation curve shows ssDNA characteristics [29]. The end-attached strand re-annealed only at zero force, since the 3rd pull cycle followed B-form curve, then a B-S transition at 60 pN, then melted at 140 pN, then relaxed again as ssDNA.*

Force-Extension Curves

Figure 16 shows seventeen superimposed stretch/release curves for a 5 kbp piece of dsDNA taken over a 5 minute period. The pipette position was measured using a light lever at a data rate of 100 Hz. Most stretch/relax curves superimpose, indicating good repeatability of force and distance measures. Fast kinetic effects are visible, such as torsionally constrained overstretching, nicked overstretching, strand melting, re-annealing and final breakage. Three instrumental problems are visible in this plot: (1) The overstretching plateau reads 60 pN rather than 65 pN, as is appropriate for dsDNA in 100 mM NaCl and room temperature. Such errors occur when dust collects on optics and light transmission is reduced below that measured when Ψ in Eq. 8 was calibrated. (2) When the molecule breaks, the force falls to –1 pN, not zero. Apparently the zero level has drifted since the last time the input light momenta were nulled, (>5 min. previous). (3) The x-axis of this plot records only the pipette position, not the molecular end-to-end distance. Therefore the apparent molecular stiffness is softened by the trap compliance, and the curves lean toward the right.

If the trap compliance (inverse stiffness) were known, it would be possible to correct for trap-bead motion and obtain the true molecular extension. Fortunately video data give us the absolute (pixel) position of the trap bead at each force, albeit with 15 nm RMS jitter. That jitter averages out over many frames, giving a good average value for the trap bead movement vs. force, i.e. the trap compliance. Thus subtracting the value (force*compliance) from each light-lever position gives the molecular extension. Force vs. light-lever extension data, corrected for (video-detected) compliance, are shown in Fig. 17.

Conclusion

The optical tweezers instrument described here is a light momentum flux sensor and actuator that makes it possible to directly exert and measure forces on objects in the range between 0.1 pN and 200 pN. Because it is a double-beam instrument, its optical alignment is both somewhat more difficult and also more crucial for its operation. On the other hand, because this instrument operates on first principles, i.e., by determining the force from a direct measurement of the change of light momentum flux, its calibration is unaffected by bead size, shape, index of refraction, and location. This feature greatly facilitates its day-to-day operation, and may make it possible to measure forces in complex refractive media such as the cell interior. When coupled to an inexpensive light lever system, this instrument can provide detailed force-extension data with a resolution of 1 nm at a bandwidth higher than 100 Hz. Sub-nanometer resolution should be possible using passive force measurement. Future improvements on vibration, sonic and thermal isolation will permit its use in the characterization of the individual steps of molecular motors such as DNA and RNA polymerases, as long as the motion is reported through a short, stiff DNA tether.

Acknowledgement: We thank Guoliang Yang for help analyzing noise spectra, Fernando Moreno and Brian Gin for help making noise/step experiments. This work was supported by grants from the National Institutes of Health, GM-32543, and the National Science Foundation, MBC-9118482 and DBI-9732140.

References

(1) A. Ashkin, *Phys. Rev. Lett.* **24**, 156-159 (1970)

(2) A. Ashkin, J. Dziedzic, J. Bjorkholm, S. Chu, *Opt. Lett.* **11**, 288 (1986)

(3) K. Svoboda and S. M. Block, *Annu. Rev. Biophys. Biomol. Struct.* **23**, 247-285 (1994)

(4) A Ashkin in "Laser Tweezers in Cell Biology" (volume 55 of Methods in Cell Biology) M. P. Sheetz ed., pp. 1-25, Academic Press, San Diego, California, 1998

(5) Simmons RM, Finer JT, Warrick HM, Kralik B, Chu S, Spudich JA. in *The Mechanism of Myofilament Sliding in Muscle Contraction,* ed. H Sugi, GH Pollack, pp. 331-336. Plenum Press, New York, NY, 1993.

(6) K. Svoboda, C. F. Schmidt, B. J. Schnapp, and S. M. Block, *Nature* **365**, 721-727 (1993)

(7) H. Yin, M. D. Wang, K. Svoboda, R. Landick, S. Block, and J. Gelles, *Science* **270**, 1653-1658 (1995)

(8) J. Happel and H. Brenner, 1991, *Low Reynolds Number Hydrodynamics* Dordecht, the Netherlands: Kluwer Academic, 2nd edition

(9) R. M. Simmons, J. T. Finer, S. Chu, and J. A. Spudich, *Biophys. J.* **70**, 1813-1822 (1996)

(10) A. Ashkin, J. M. Dziedzic and T. Yamane, *Nature* **330**, 769-771 (1987)

(11) M. W. Berns, W. H. Wright, B. J. Tromberg, G. A. Profeta, J. J. Andrews, and R. J. Walker, *Proc. Natl. Acad. Sci. USA*, **86**, 4539-4543 (1989)

(12) S. B. Smith, Doctoral Thesis, University of Twente, Netherlands, October 16, 1998

(13) S. B. Smith, Y. Cui, and C. Bustamante, *Science* **271**, 795-798 (1996)

(14) C. G. Baumann, V. Bloomfield, S. B. Smith, C. Bustamante, M. Wang, S. Block, *Biophys. J.* **78**, 1965-1978 (2000)

(15) M. S. Z. Kellermayer, S. B. Smith, H. L. Granzier, C. Bustamante, *Science*, **276**, 1112 - 1116 (1997)

(16) M. Hegner, S. B Smith C. Bustamante, *Proc. Nat. Acad. Sci. USA* **96**, 10109-10114 (1999)

(17) Y. Cui and C. Bustamante, *Proc. Nat. Acad. Sci. USA* **97,** 127-132 (2000)

(18) G. Wuite, S. B. Smith, M. Young, D. Keller, C. Bustamante, *Nature*, **404**, 103-106 (2000)

(19) J. Liphardt, B. Onoa, S. B. Smith, I. Tinoco Jr., C. Bustamante, *Science* **292**, 733-737 (2001)

(20) D. E. Smith, S. Tans, S. B. Smith, S. Grimes, D.L. Anderson, C. Bustamante, *Nature* **413**, 748-752 (2001)

(21) J. P. Gordon, *Phys. Rev. A* **8**, 14-21 (1973)

(22) M. Pluta, *Advanced Light Microscopy* ,volume 1, page 163, Eq. 2.34c, Elsevier, Amsterdam 1988

(23) L. P. Ghislain, N. A. Switz and W. W. Webb,*Rev. Sci. Instrum.* **65**, 2762-2768 (1994)

(24) M. Allersma, F. Gittes, M. J. deCastro, R. J. Stewart, C. F. Schmidt, *Biophys. J.* **74**, 1074-1085 (1998).

(25) T. N. Buican, in *Am. Chem. Soc. Symp.* **464**, *Cell Separation Science and Technology*, D. S. Kompala and P. T. Todd, eds. (1991)

(26) M. C. Wang, G. E. Uhlenbeck, *Rev. Mod Phys.* **17**, 323-341 (1945); Reprinted in *Selected Papers on Noise and Stochastic Processes*, ed. N. Wax, pp. 113-132. New York, NY: Dover

(27) W. H. Wright, G. J. Sonek and M. W. Berns, *Applied Optics* **33**, 1735-1748 (1994)

(28) P. Cluzel, A. Lebrun, C. Heller, R. Lavery, J-L Viovy, D. Chatenay and F. Caron, *Science* **271**, 792-794 (1996)

(29) S. B. Smith, Y. Cui, and C. Bustamante, *Science* **271**, 795-798 (1996)

(30) W. Denk and W.W.Webb*, Appl. Optics* **29**, 2382-2390 (1990)

(31) C. Bustamante, C. Rivetti and D. J. Keller, *Current Opinion in Structural Biology*, **7**, 709-716 (1997)

(32) C. Bustamante, J. F. Marko, E. D. Siggia and S. B. Smith, Science 265, 1599-1600 (1994)

(33) C. Bouchiat, M. D. Wang, J.-F. Allemand, T. Strick, S. M. Block, and V. Croquette**,** *Biophys. J.* **76**: 409-413 (1999)

(34) J. F. Leger, G. Romano, A. Sarkar, J. Robert, L. Bourdieu, D. Chatenay and J. F. Marko, *Phys. Rev. Lett.* **83**, 1066-1069 (1999)

(35) H. Clausen-Schaumann, M. Rief, C. Tolksdorf, and H. E. Gaub, *Biophys. J.* **78**, 1997-2007 (2000)